



Special Feature: Automotive Exhaust Catalyst

Research Report

Atomic-level Analysis and Catalytic Activity of Size-selected Pt Clusters Deposited on TiO₂(110)

Yoshihide Watanabe, Noritake Isomura, Hirohito Hirata and Xingyang Wu

Report received on Jan. 20, 2011

■ **ABSTRACT** ■ A new experimental setup to study catalytic and electronic properties of size-selected clusters on metal oxide substrates for developing heterogeneous catalysts, such as automotive exhaust catalysts, has been developed. The apparatus consists of a size-selected cluster source, a photoemission spectrometer, a scanning tunneling microscope (STM), and a high-pressure reaction cell. The high-pressure reaction cell measurements provide information on catalytic properties under conditions close to those in practical uses. We investigated size-selected Pt_n ($n = 4, 7-10, 15$) clusters deposited on TiO₂(110) under soft-landing conditions. The catalytic activity measurements showed that the catalytic activities have a cluster size dependence. We obtained atomic-resolution images of size-selected clusters on surfaces, enabling the identification of atomic alignment in the clusters. Clusters smaller than Pt₇ lay flat on the surface with a planar structure, and a planar-to-three-dimensional (3D) transition occurred at $n = 8$ for Pt_n clusters on TiO₂. The binding energies of Pt 4f_{7/2} decreased steeply with increasing cluster size up to $n = 7$ for Pt_n, and decreased gradually for $n \geq 8$. This inflection point ($n = 8$) agrees well with the cluster size at the planar-to-3D transition. It was found that the core-level shifts of size-selected Pt clusters on TiO₂ are closely correlated with cluster geometries.

■ **KEYWORDS** ■ Cluster, Mass-selected, Size-selected, Scanning tunneling microscopy (STM), Reaction, TiO₂(110), Platinum, CO, Oxidation, Deposition

1. Introduction

Heterogeneous catalysts, such as those used in automotive exhaust systems, consist of precious metal particles supported on oxide surfaces. Currently, there is a real and urgent need to reduce precious metal usage. It is speculated that the catalytic activity of metal clusters has a strong size-dependence. Clusters on a surface would provide further specificity because of the interaction between the clusters and the surface. To study the catalytic and electronic properties of size-selected clusters on metal oxide substrates from the view point of cluster-support interaction, as well as to devise a method for controlling catalytic activity and thermal stability, an experimental setup has been developed. Cluster size and cluster-support interactions are key parameters that control catalytic activity and thermal stability of a cluster catalyst.

There have been a number of studies on the catalytic properties of free size-selected clusters; however, few studies have been conducted on the catalytic properties of surface-deposited size-selected clusters. This dearth of studies is mainly due to the difficulty in preparing

well-defined uni-sized clusters on a surface for comparison with those deposited using a cluster beam method. Some studies have been carried out on systems wherein size-selected clusters have apparently been deposited successfully without fragmentation or aggregation.

Heiz et al. developed the first instrument that allowed for detailed study of the chemical properties of size-selected deposited clusters using the temperature programmed desorption (TPD) method⁽¹⁾; they also reported that the catalytic activity of size-selected Pt_n ($n = 5-20$) clusters on MgO(100) films in the oxidation of carbon monoxide increased abruptly during the transition from Pt₈ to Pt₁₅.^(2,3) A similar investigation of Au_n ($n = 1-7$) clusters on TiO₂(110) by Lee et al.⁽⁴⁾ showed that catalytic activity increased substantially for Au₆ and Au₇. Although these two studies show strong dependence of catalytic activity on the deposited cluster size, the geometries of the metal clusters on the surfaces were not measured directly in either case. In the case of single crystal metal surfaces, the catalytic activity was different on different crystal faces of the same metal⁽⁵⁻⁷⁾ as well as

on different sites of the same crystal face.⁽⁸⁾ This suggests that the catalytic activity may depend on the alignment of the atoms in the clusters. Tong et al.⁽⁹⁾ investigated the shapes and sizes of size-selected Au_n (*n* = 1-8) clusters on TiO₂(110) using scanning tunneling microscopy (STM). The alignment of gold atoms in the clusters was not identified clearly in the reported STM images. On the other hand, Piednoir et al.⁽¹⁰⁾ showed atomic-resolution images of palladium clusters on surfaces but the clusters were not size-preselected. In both cases, it is difficult to discuss the origin of the strong size dependence of catalytic activity of clusters on surfaces.

We present a new experimental setup to study the specificity of size-selected clusters on a surface. The setup combines a mass-selective cluster deposition source with an X-ray photoelectron spectrometer, ultraviolet photoelectron spectrometer, STM, and a high-pressure reaction cell. The high-pressure reaction cell measurements provided information on catalytic properties under conditions close to those used in practical applications. We chose TiO₂(110) as the initial support for the study because it is one of most popular metal oxides and it is conductive after a typical cleaning procedure, which allows it to be deposited without charge built-up and to be studied by STM.

The surface structures and electronic properties of TiO₂(110) surfaces were studied by various surface-sensitive techniques, including X-ray photoelectron spectroscopy (XPS),^(11,12) ultraviolet photoelectron spectroscopy (UPS),^(13,14) and STM.^(15,16) We have studied Mass-selected Pt clusters deposited on TiO₂(110) surfaces in recent years.^(17,18)

We investigated the geometries of size-selected Pt clusters deposited on TiO₂(110) surfaces. In the STM measurements described here, a carbon nanotube (CNT) STM tip that can provide atomic-resolution⁽¹⁹⁾ images was used to image the alignment of the Pt atoms in the clusters. The high aspect ratio of the CNT tip enables imaging at a high lateral resolution, especially on surfaces with steep changes in height, e.g., clusters on a surface. The catalysts were characterized by XPS, and core-level shifts of the supported nanoclusters were often observed.^(20,21) The core-level shift is of great interest because it reflects cluster-surface interactions that affect catalytic activities.⁽²²⁾ Most previous studies on supported metal nanoclusters by photoelectron spectroscopy were carried out on evaporated or sputtered thin films,⁽²³⁻²⁷⁾ where the average cluster size distribution was

estimated from other observations. Recently, the relation between cluster size and core-level shifts have been studied using size-selected metal clusters deposited on surfaces.⁽²⁸⁻³¹⁾ Although these studies show strong size dependence of the core-level shifts, the geometries of the clusters on the surfaces were not measured directly. This makes it difficult to discuss the origin of the strong size dependence.

In this paper, we report the geometries and size dependence of size-selected Pt_n (*n* = 4, 7-10, 15) clusters deposited on TiO₂(110)-(1×1) surfaces at room temperature in ultrahigh vacuum (UHV). Alignments of the Pt atoms in the clusters are imaged at atomic resolution using the CNT STM tip. Size distributions of the clusters on the surfaces are measured as a function of the size of the deposited clusters. Further study by XPS makes it possible to distinguish the correlation between cluster geometries and core-level shifts.

2. Experimental

Figure 1 shows an overview of the experimental setup used in this study, and **Fig. 2** shows a schematic of the setup. The apparatus combines a cluster source, ion optics, quadrupole mass filter, deposition stage, reaction cell, and surface analysis systems. All the chambers are connected to each other, and the sample was transferred under UHV conditions to investigate as-deposited clusters on the surface. The deposition, STM observation, and transfer between the deposition chamber and STM chamber can be performed under cryogenic temperatures to freeze the movement of the deposited clusters. We deposited size-selected Pt clusters on TiO₂(110) surfaces prepared by the typical procedure by using a new UHV cluster deposition apparatus with a magnetron-sputter ion source.

The deposited Pt clusters and TiO₂ surfaces were observed by STM. This system was also equipped with low-energy electron diffraction (LEED)/Auger electron spectroscopy (AES), XPS, and UPS (see Fig. 2).

The experimental details will be elaborated in each section.

2.1 Sample preparation

We used 10 mm × 10 mm TiO₂(110) single crystals for the deposition.

The samples for the experiments were prepared by Pt_n⁺ deposition on rutile TiO₂(110) single crystals (10

$\times 10 \text{ mm}^2$, Shinkosha Co., Ltd). Prior to the deposition, the $\text{TiO}_2(110)$ surfaces were cleaned by repeated cycles of Ar^+ sputtering (1 keV, 10 min) and annealed at 980 K in vacuum, until a well-defined (1×1) LEED pattern was observed and no impurities were detected by AES. This treatment also creates bulk oxygen vacancies, making the sample surfaces sufficiently conductive for ion deposition with minimal charging.

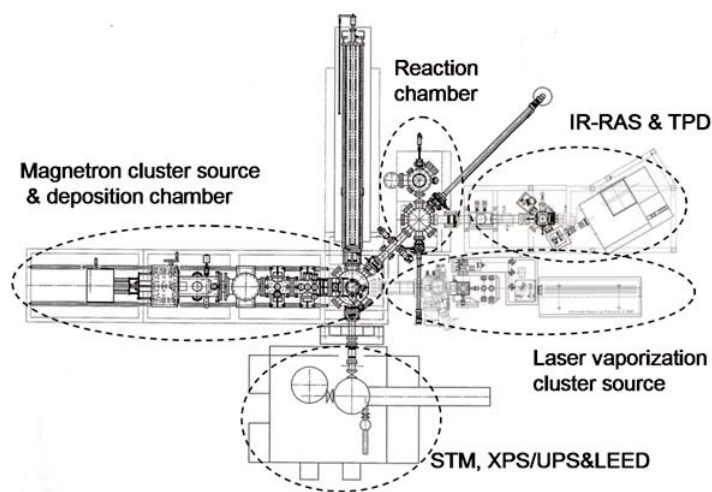


Fig. 1 Overview of the experimental setup.

2.2 Cluster source and deposition

Figure 3 shows a schematic view of the cluster source. Metal clusters were produced by magnetron sputtering and gas condensation.⁽³²⁾ Energetic metal atoms sputtered from the target were cooled by He gas, leading to nucleation of clusters. After expansion through a nozzle, the ionized clusters were accelerated and focused by an ion funnel. The cluster beam was then mass-selected by an Extrel quadrupole mass filter (Extrel MEXM-4000, mass range of 1-4000 amu) and finally deflected to the substrate or to another quadrupole mass analyzer.

The magnetron sputtering source was built with a commercially available magnetron (Angstrom Sciences Inc., ONYX-1). The distance between the sputtering-target plate ($\phi 50 \text{ mm}$) and an exit aperture of the aggregation chamber was adjusted to optimize the intensity and size distribution of the targeted metal cluster ions.

The ion funnel⁽³³⁾ was mounted on the exit aperture plate of the aggregation chamber, allowing for easy removal for cleaning. When ions are introduced into the mouth of the funnel, the DC potential drives them toward the exit while the effective RF field prevents ions from hitting the electrodes. The net effect is to capture the entire

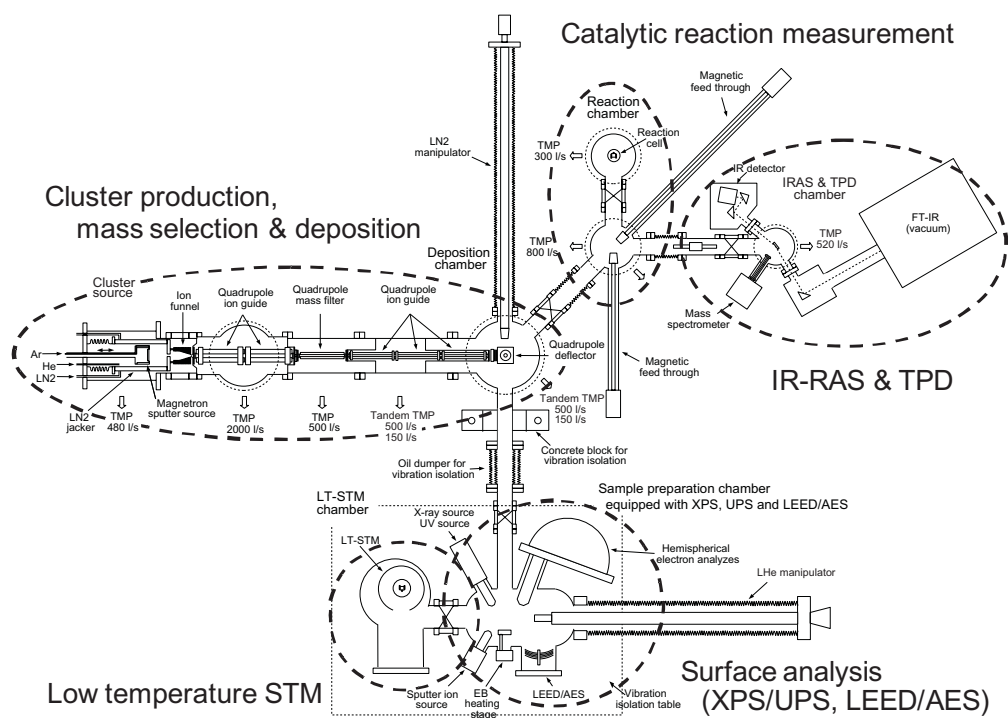


Fig. 2 Schematic of the experimental setup.

expanding ion cloud and then to focus the ions towards the next ion guide. At the same time, collisions with ambient gas dampens the motion of the ions, resulting in a narrow kinetic energy distribution at the end of the funnel. The ion funnel reduces ion escape due to scattering by He atoms. Driving potentials were applied to each electrode. A resistor chain on each electrode worked as a DC voltage divider. The ring electrodes had a continuously decreasing DC bias (for positive ions) towards the bottom of the ion funnel electrode stack. Typical DC biases applied to the ion funnel were 10-80 V for the last ring electrode. RF potentials were applied in phase to odd-numbered ring electrodes and 180° out of phase to even-numbered electrodes. The RF signal was generated by an RF generator (WF1943A, NF Corporation) and amplified by an RF amplifier (BA4825, NF Corporation).

Platinum cluster ions were deflected by 90° by a quadrupole deflector to remove neutral clusters that were not mass-selected. The cluster ions, with a flux of 0.01-2 nA/cm², were deposited on TiO₂(110) single-crystal surfaces at room temperature under soft landing conditions. The impact energy of the clusters onto the surfaces, measured using retarding potential analysis of the substrate, was tuned to less than 2 eV/atom by adjusting the voltage and frequency applied to the ion funnel as well as the voltage applied to the ion deflector. The platinum coverage was 5 × 10¹³ to 1 × 10¹⁴ atoms/cm², corresponding to approximately 5-10% of a closed-packed platinum monolayer. The ambient pressure was less than 1 × 10⁻⁷ Pa during deposition.

We deposited the size-selected Pt clusters on

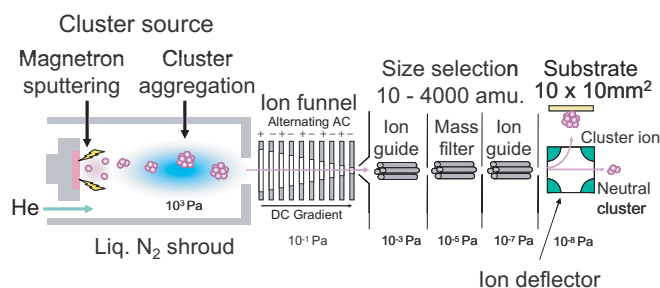


Fig. 3 Schematic view of the experimental set-up for the production of size-selected metal clusters. (Clusters are produced by DC magnetron sputtering with liquid nitrogen cooling, an ion funnel, mass-selection, deflection, and einzel lenses to focus the cluster beam.)

TiO₂(110) surfaces using a new UHV cluster deposition apparatus with a magnetron-sputter ion source. Energetic metal atoms sputtered from the target were cooled by He gas, yielding nucleation of the clusters. Ar and He pressures were adjusted to tune the distribution of available cluster sizes. The translational energy of the cluster ions in these ion-guides was adjusted to be less than 0.5 eV/atom by applying appropriate DC voltages to each center of the RF voltage.

2.3 Reaction cell

Figure 4 gives a schematic view of the reaction cell. The high-pressure reaction cell was designed for studies of catalytic activity at high pressures using small-area samples and a retractable internal isolation cell with a quartz lining, which constitutes a micro-batch reactor in the ~20 kPa pressure range under conditions close to those in practical use. The reaction cell and external recirculation loop were connected to a stainless steel bellows pump (Senior Aerospace MB-158HT) for circulation.

The sample was heated by an infrared radiation heating system (GVH298, THERMO RIKO Co., Ltd.) wherein the infrared radiation was transmitted from the heating source on the atmospheric side through a quartz rod. The temperature was measured with a thermocouple. The test temperature was increased step by step.

Recirculation of the reaction gas compensated for the low concentration of active sites. A quadrupole mass spectrometer was used to analyze the reaction gas, in combination with gas chromatography when required.

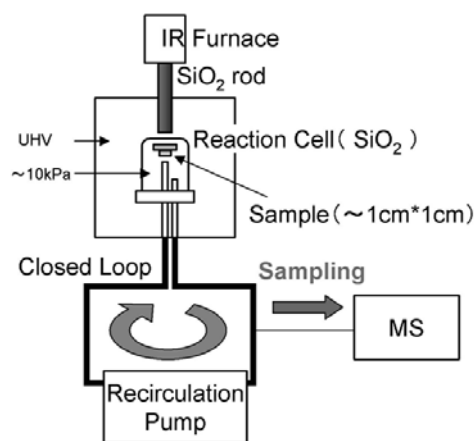


Fig. 4 Schematic of the high-pressure reaction cell.

2.4 STM observations

STM observations were carried out using a low-temperature STM (Omicron LT-STM) attached to a surface analysis chamber.

The samples were imaged by STM using the CNT tip. STM images of the surface were acquired at 80 K in a constant current mode using a low-temperature STM (Omicron NanoTechnology GmbH) with a Nanonis controller (SPECS Zurich GmbH).

Typical operating parameters included sample bias in the range from +1 to +3 V and a tunneling current of 0.05-0.1 nA. The CNT tip for STM was supplied by Yoshimura (Toyota Technological Institute) and fabricated by manually attaching a CNT to the tip apex using electron-beam-induced deposition of amorphous carbon under a scanning electron microscope.

The sample preparation and transfer were carried out under cryogenic temperatures using a liquid He cooled manipulator. Vibration isolation was achieved with a spring suspension with eddy current dampers. The STM chamber was also isolated by air suspension. For isolation from vibration of the deposition chamber, the transfer chamber between the deposition chamber and the surface analysis chamber was tightly held by a concrete block panel and separated by an oil damper in-between. Image processing was performed using the Nanotec WSxM⁽³⁴⁾ software. The base pressure of the STM chamber was less than 1×10^{-8} Pa.

2.5 Surface analysis

The surface analysis chamber (μ -metal) was equipped with LEED/AES, a hemispherical analyzer (Omicron EA125HR), a Mg/Al twin anode X-ray source (Omicron DAR400), a VUV light source (Omicron HIS13), an ion gun, e-beam and resistive heating systems, an IR thermometer (Japan sensor FTZ6), and a gas doser.

The samples were characterized by XPS (Omicron NanoTechnology GmbH) using Mg K α (1253.6 eV) radiation from a dual-anode X-ray source, together with a hemispherical energy analyzer and a seven-channel detector. XPS spectra were taken at an electron take-off angle of 40° with a pass energy of 20 eV. The spectra were calibrated so that the Ti 2p_{3/2} peak appeared at 459.0 eV of the binding energy expected for bulk TiO₂.⁽³⁵⁾

2.6 Pulsed laser vaporization cluster source and FT-IRAS

Another cluster source using the pulsed laser vaporization method was also used. Fourier transform infrared reflection-absorption spectroscopy (FT-IRAS) was used for gas adsorption analysis. Details will be reported in the near future.

3. Results and discussion

3.1 Cluster production and deposition

Figure 5 shows a typical distribution of the Pt cluster ion current. The total current of the Pt cluster ions was typically 200 nA, whereas the typical mass-selected cluster ion current was 1-50 pA.

Typically, 3×10^{11} atoms ($6-13 \times 10^{10}$ of size-selected cluster ions) were deposited on a 10 mm-diameter circular area on the surface by adjusting the current of the cluster-ion beam and the deposition time under a pressure of 6×10^{-8} Pa at 300 K. The current and deposition time were 5-50 pA and 100-600 s, respectively. The collision energy of the cluster ions against the surface was less than 0.5 eV per platinum atom. Cluster ions after size selection were deposited onto a TiO₂(110) surface at a collision energy, E_{col} , of 0.25 eV per Pt atom (the translational energy of the cluster ions was <1.9 eV (~ 0.25 eV/atom)). The uncertainty in the collision energy (full width at half maximum, FWHM) was 0.4-1 eV per platinum atom.

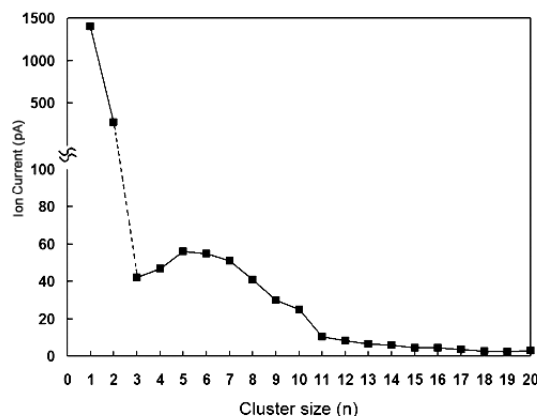


Fig. 5 Ion current distribution of Pt clusters after deflection.

3.2 Catalytic activity measurements

Catalytic oxidation of CO on size-selected Pt clusters on a TiO₂(110) surface was investigated using a high-pressure reaction cell. The test temperature was increased step by step. At each temperature, the reaction rate of CO oxidation was constant, as shown in Fig. 6. As the temperature increased, the reaction rate also increased. These results indicated that the CO oxidation reactions in this reactor were properly observed.

As shown in Fig. 7, the reaction rates of CO oxidation on the size-selected Pt clusters deposited on TiO₂(110) were measured for each cluster size from monomer to heptamer. The normalized production rates of CO₂ by the number of Pt atoms on the sample show cluster-size dependence. These results are

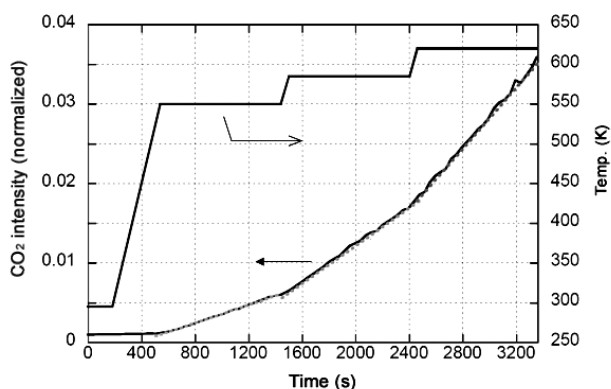


Fig. 6 CO₂ concentration of the CO oxidation reaction over Pt₈/TiO₂(110) at the programmed temperature.

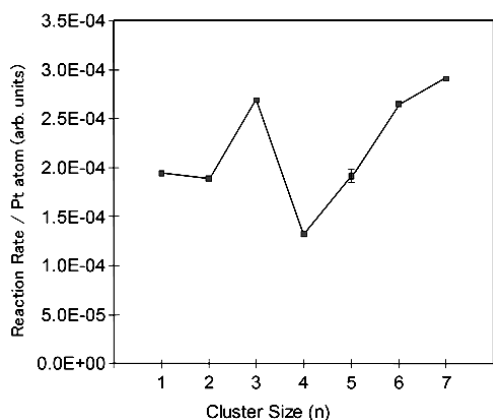


Fig. 7 CO oxidation activity on Pt_n/TiO₂(110).

preliminary and we plan to show and discuss further results in an upcoming report in the near future.

3.3 STM observation

The deposited Pt clusters and TiO₂ surfaces were observed using STM. Figure 8 shows STM images of a clean TiO₂(110)-(1×1) surface consisting of terraces ~100 nm wide and steps ~0.3 nm high; the latter value agrees with the expected step height for a rutile TiO₂(110)-(1×1) surface.⁽³⁶⁾ The bright and dark lines visible in Fig. 8(b) were assigned to fivefold coordinated titanium atom rows and bridging oxygen atom rows, respectively. They were separated by approximately 0.65 nm, which is in agreement with the previously reported value.⁽³⁷⁾ The bright spots between the titanium rows correspond to vacant sites in the bridging O rows, as shown by Wendt et al.⁽³⁸⁾

Figure 9 shows STM images after deposition of size-selected Pt_n (n = 4, 7-10, 15) cluster ions. In Figs. 9(A)-9(F), the observed bright spots were assigned to size-selected clusters because the number of spots agrees reasonably well with the value estimated from the current of the cluster ions, and also the sizes of the spots were almost the same. The deposited Pt clusters were not observed to sit on specific sites relative to the TiO₂ lattice in any size, suggesting that they were randomly positioned. No fragmentation was observed for any size cluster either. These clusters were determined to be attached firmly to the TiO₂ surface without aggregation, because the STM images did not change in repeated scans. Figures 9(a)-9(c) and 9(c'), Figs. 9(d) and 9(d'), and Figs. 9(e) and 9(f) show images of a specific cluster in each case at atomic resolution. Height distributions and average heights of

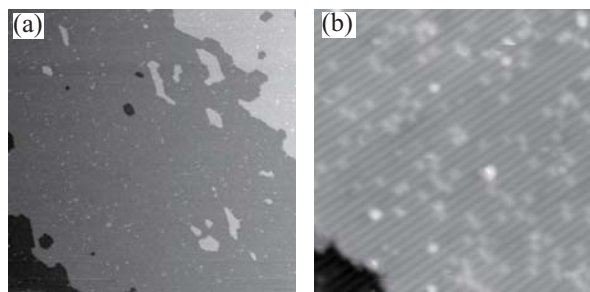


Fig. 8 [(a) and (b)] STM images of a clean surface of titanium dioxide, with (b) oxygen vacancies visible between fivefold coordinated titanium atom rows. (a) The left image is 200 × 200 nm² and (b) the right one is 20 × 20 nm².

the clusters are shown in **Figs. 10** and **11**, respectively. Figures 9(A) and 9(a) and Figs. 9(B) and 9(b) show STM images taken after deposition of Pt_4^+ and Pt_7^+ , respectively. Pt_4 and Pt_7 clusters were clearly seen to consist of four and seven platinum atoms, respectively [Figs. 9(a) and 9(b)]. Height distributions of the Pt_4 and Pt_7 clusters on the surfaces were narrow [Figs. 10(a) and 10(b)], suggesting that both clusters had only a planar structure and lay flat on the surface.

Figures 9(C), 9(c), and 9(c') show STM images obtained after deposition of Pt_8^+ . One platinum atom was clearly identified in Fig. 9(c) and was assigned to the second atomic layer from its height of 0.5 nm, corresponding to approximately 2 times the diameter of a platinum atom. In other words, the Pt_8 cluster was assumed to be a geometric structure consisting of one atom on the first layer with seven atoms below.

Figures 9(D), 9(d), and 9(d') show STM images obtained after deposition of Pt_9^+ . Two platinum atoms can be clearly identified in Fig. 9(d) and were assigned to the second atomic layer. That is, the Pt_9 cluster was assumed to be a geometric structure consisting of two atoms on the first layer with seven atoms below. In

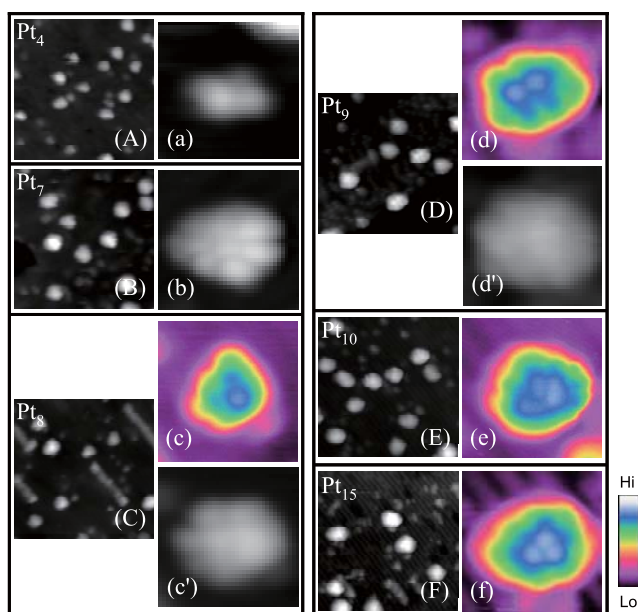


Fig. 9 STM images of a $\text{TiO}_2(110)$ surface after deposition of size-selected Pt_n^+ ($n = 4, 7-10, 15$) cluster ions. Images with uppercase letters are $20 \times 20 \text{ nm}^2$ and those with lowercase letters are $3.5 \times 3.5 \text{ nm}^2$ views of one cluster on the same surface. [(A)(a)] The TiO_2 surface after the deposition of Pt_4^+ , [(B)(b)] Pt_7^+ , [(C)(c)(c')] Pt_8^+ , [(D)(d)(d')] Pt_9^+ , [(E)(e)] Pt_{10}^+ , and [(F)(f)] Pt_{15}^+ . A color scale indicates heights for (c)-(f).

Figs. 9(c') and 9(d'), Pt_8 and Pt_9 clusters were assumed to have a planar structure on the basis of their height, approximately 0.35 nm. Pt_8 and Pt_9 clusters were dimly observed to consist of eight and nine Pt atoms, respectively. In contrast to the Pt_4 and Pt_7 clusters, the height distributions of the Pt_8 and Pt_9 clusters were

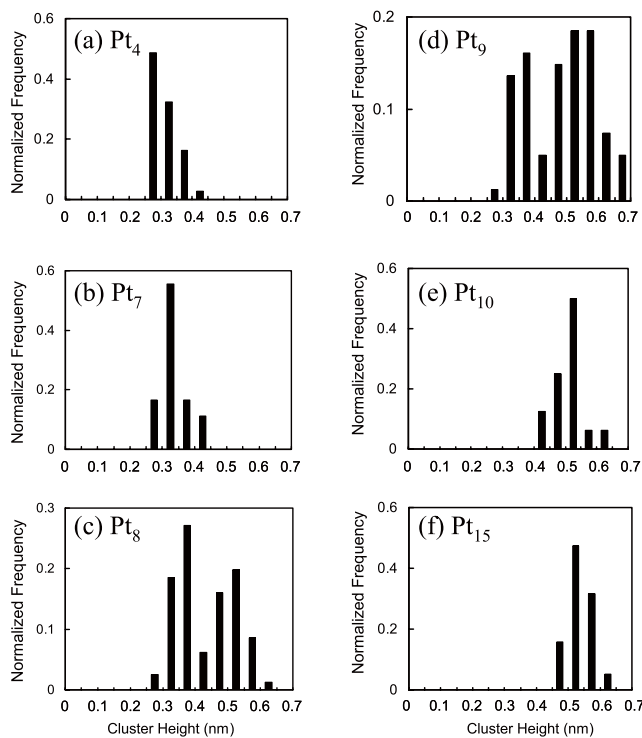


Fig. 10 Cluster height distributions of deposited Pt_n ($n = 4, 7-10, 15$) on $\text{TiO}_2(110)-(1 \times 1)$ surfaces.

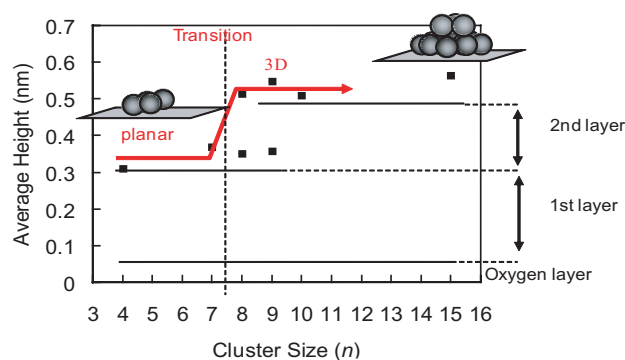


Fig. 11 Average cluster heights for Pt_n ($n = 4, 7-10, 15$) on the $\text{TiO}_2(110)-(1 \times 1)$ surface. The two heights in Pt_8 and Pt_9 correspond to two separate peaks in the height distributions. The long-dashed line represents the height of the invisible bridging oxygen atom relative to the visible titanium atom at zero. The short-dashed lines indicate heights expected for various platinum layers in the cluster.

separated into two peaks [Figs. 10(c) and 10(d)]. The average height of each peak was approximately 0.35 and 0.53 nm for both cluster sizes (Fig. 11), indicating two types of geometric structures. It was found that the shorter clusters lay flat on the surface with a planar structure, whereas the taller ones had a three-dimensional (3D) structure with two atomic layers.

Free platinum clusters of up to nine atoms with a planar structure are as stable as their 3D isomers, as indicated by density functional theory (DFT) calculations.⁽³⁹⁾ It is suggested that Pt₈ and Pt₉ clusters could have two types of structures in the gas phase before deposition. Figures 9(E) and 9(e) and Figs. 9(F) and (f) show STM images obtained after the deposition of Pt₁₀⁺ and Pt₁₅⁺, respectively. Three platinum atoms were clearly identified in Fig. 10(f) and were assigned to the second atomic layer on the basis of their height, 0.5 nm. That is, the Pt₁₅ cluster was assumed to be a geometric structure consisting of 3 atoms on the first layer with 12 atoms below. Figures 10(e) and 10(f) show height distributions for the Pt₁₀ and Pt₁₅ clusters, respectively. In contrast to Pt₈ and Pt₉, the distributions of Pt₁₀ and Pt₁₅ clusters had only one peak, suggesting that both of these size clusters had only 3D structures with two atomic layers. In STM images of Pt₄ and Pt₇, the distances between adjacent bright spots in each cluster were observed to be approximately 0.7 nm [Figs. 9(a) and 9(b)]. This is longer than the Pt–Pt bond length in bulk and is also longer than that of free platinum clusters, which ranges from 0.24 to 0.29 nm in the size range of 3–55, as shown by discrete Fourier transform calculation.⁽³⁹⁾ Schoiswohl et al.⁽⁴⁰⁾ showed that one vanadium atom and neighboring oxygen atoms were observed together as one bright spot in the

case of planar vanadium oxide V₆O₁₂ clusters. Their results suggest that one Pt atom in a cluster and one or more nearby oxygen atoms of TiO₂, bound together by strong interactions,⁽⁴¹⁾ might be observed together as one bright spot in our experiments. In soft-landed Au clusters on TiO₂(110)–(1×1) surfaces investigated by Tong et al.,⁽⁹⁾ the distance between bright spots in a Au₄ cluster on the surface was seen to be approximately 0.7 nm. In the case of Pt and Au clusters on TiO₂, metal-metal bond lengths might be elongated.

It was found that clusters smaller than Pt₇ on a TiO₂(110)–(1×1) surface lay flat on the surface with a planar structure, and a planar-to-3D transition occurred at $n = 8$ for Pt_{*n*} on TiO₂. This transition also occurred for Au_{*n*} on TiO₂ with $n = 5$.⁽⁹⁾ DFT calculations of free clusters showed that the binding energies for both Pt and Au clusters increased with cluster size.^(39,42) Strong interaction with TiO₂ surfaces could result in planar structures for smaller clusters because the binding energies are lower in smaller clusters. The value of the binding energy in the size range of 5–8 was larger than 2.8 eV for Pt_{*n*}⁽³⁹⁾ and was less than 2.1 eV for Au_{*n*}.⁽⁴¹⁾ The geometric transition size of Pt clusters is considered to be larger than that of Au clusters because the binding energy of Pt clusters is larger than that of Au clusters. It is suggested that the geometries of clusters on the surfaces could be affected by the relationship between the strength of metal-metal bonds in the clusters and interactions with the surface.

3.4 Photoelectron spectroscopy

Figure 12 shows XPS spectra for a clean TiO₂ surface as well as TiO₂ surfaces with size-selected,

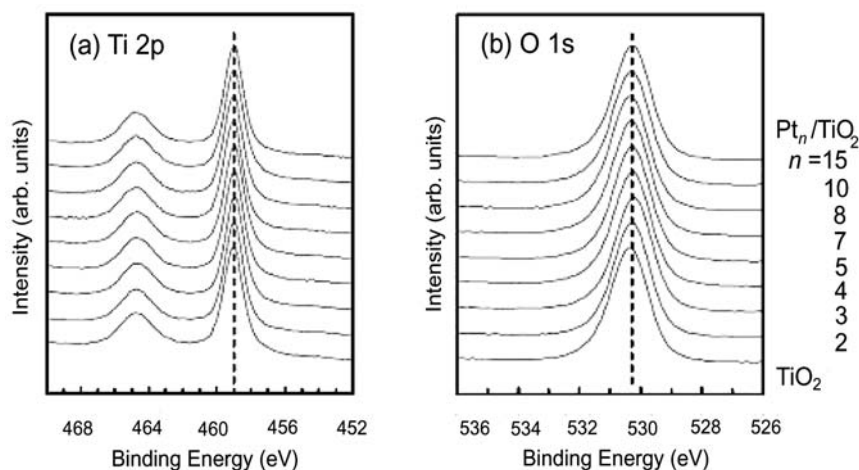


Fig. 12 (a) Ti 2p and (b) O 1s XPS spectra of TiO₂ surfaces with mass-selected, deposited Pt_{*n*} ($n = 2-5, 7, 8, 10, 15$) and a clean TiO₂(110) surface (bottom spectrum). Peak positions are indicated by vertical dotted lines.

deposited Pt_n ($n = 2-5, 7, 8, 10, 15$) (Pt_n/TiO_2). For the clean surface, a Ti^{3+} shoulder at approximately 2 eV lower than the dominant Ti^{4+} peak⁽⁴³⁾ was not observed in the Ti 2p region. This suggests that the clean TiO_2 surface has relatively fewer missing oxygen defects. The Ti 2p and O 1s spectra for Pt_n/TiO_2 are similar to those for the TiO_2 surface without Pt clusters, and the Ti^{3+} shoulder in the Ti 2p region was also not observed after Pt deposition. Pt 4f spectra for size-selected Pt_n ($n = 2-5, 7, 8, 10, 15$) deposited on TiO_2 are shown in **Fig. 13**. Here, Pt 4f core-level shifts were observed, and the binding energies of the Pt 4f peak decreased with increasing cluster size. Regardless of the shift in the Pt 4f peaks, the peaks had no shoulder, and their widths were almost constant. These results indicate that one peak with no other component shifted with increasing cluster size. The electronic states for most of the dispersed Pt clusters, at least as observed by XPS, were almost the same at each size. The cluster size dependence of binding energies of the Pt $4f_{7/2}$ peak is shown in **Fig. 14**. The binding energy of the peak decreased steeply with increasing cluster size up to $n = 7$ for Pt_n and then decreased gradually. This decreasing tendency of the core-level shifts for Pt_n/TiO_2 is similar to that for the Pd clusters on TiO_2 reported by Kaden et al.,⁽³¹⁾ who showed that the core-level shifts were correlated with the cluster geometries estimated by low-energy ion scattering spectroscopy.

The above-mentioned steep binding energy shift for clusters smaller than Pt_7 could occur because the clusters grew in the plane with increasing cluster size, and the number of Pt atoms contacting the TiO_2 surface

increased by one atom. In contrast, for clusters larger than Pt_8 , the number of Pt atoms in the first layer contacting the TiO_2 surfaces was observed to increase by only a few with cluster sizes up to at least Pt_{10} as estimated from the cluster geometries.⁽¹⁷⁾ This small increase could cause the gradual binding energy shift for clusters larger than Pt_8 , as mentioned above. The configuration or coordination of Pt atoms would also contribute to the binding energy, and gradual changes might result in the shift of the binding energy. The cluster size dependence of the core-level shifts can be interpreted in terms of the influence of the cluster geometry on cluster-surface interactions. Note that such shifts result from a combination of initial- and final-state effects,⁽⁴⁴⁾ but based on photoemission results alone, we cannot unambiguously differentiate between them. Nevertheless, artifacts such as charging effects must be excluded. One problem with such samples (i.e., small particles on insulating surfaces) is differential charging.⁽⁴⁵⁾ This is excluded here because the surfaces in this study would be conductive as a result of sputtering and annealing. The peak widths are small and show no broadening, which is a clue to the absence of charging effects.

The lowest binding energy of the Pt clusters was approximately 71.6 eV at Pt_{15} (Fig. 14). This value is higher than the 71.2 eV for the bulk metal.⁽²⁹⁾ Many of the atoms at the reconstructed (1×1) surfaces are oxygen, as is well known.^(19,20) We suppose that Pt–O bonds would be formed, and the Pt clusters would not be in metallic states. The Pt 4f spectra in Fig. 13 do not exhibit characteristic asymmetry observed for bulk

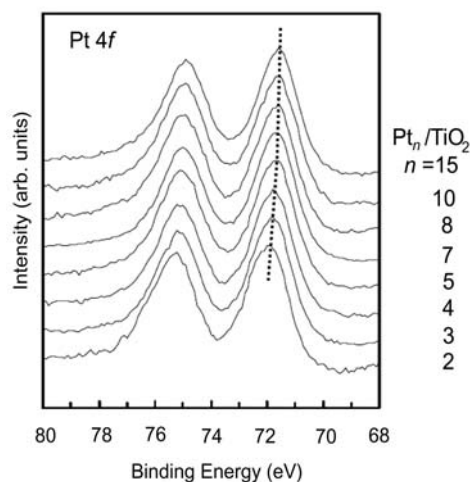


Fig. 13 Pt 4f XPS spectra for mass-selected Pt_n ($n = 2-5, 7, 8, 10, 15$) deposited on $TiO_2(110)$. The peak position is indicated by the vertical dotted line.

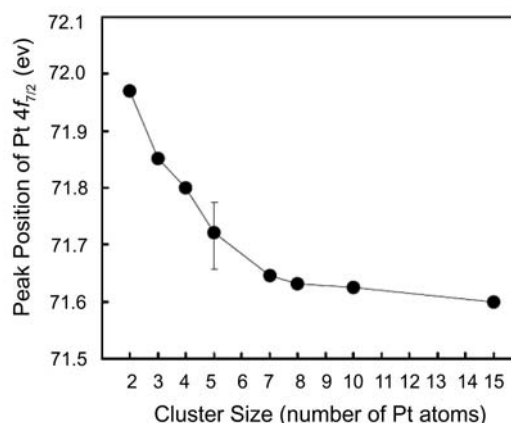


Fig. 14 Binding energies of the Pt $4f_{7/2}$ peak for mass-selected Pt_n ($n = 2-5, 7, 8, 10, 15$) on $TiO_2(110)$ surfaces as a function of cluster size.

metal,⁽⁴⁶⁾ supporting the existence of nonmetallic states. Eberhardt et al.⁽²⁹⁾ measured valence-band spectra for Pt clusters on SiO₂ and discussed nonmetallic states in detail. Although we did not obtain valence-band spectra, the nonmetallic states of Pt clusters could be explained roughly by the XPS results. On the other hand, the highest binding energy of the Pt clusters was approximately 72.0 eV for Pt₂ (Fig. 14); that is, the maximum shift relative to the bulk metal was approximately 0.8 eV. The core-level shifts for various Pt oxides and hydroxides are well known,⁽⁴⁶⁾ typically being approximately 3 eV for stoichiometric compounds. This value is significantly larger than the maximum shift observed in this study, indicating that only stoichiometric oxides will not be formed in all sizes of the Pt clusters on TiO₂ surfaces, because the Pt 4f spectra do not exhibit a multiple-peak substructure or significant broadening. Thus, intermediate core-level shifts between metal and stoichiometric oxides are thought to occur in Pt clusters on TiO₂ because Pt–O bonds would be formed. Furthermore, stoichiometric oxides would not be formed yet. Moreover, we believe that Pt–Pt bonds were not broken in the Pt clusters on TiO₂. If the Pt–Pt bonds were broken, isolated Pt atoms would be expected to sit on the reconstructed (1×1) surfaces with relatively many oxygen atoms, and core-level shifts corresponding to Pt oxides would then be observed. However, the observed core-level shifts are in fact far from the value for Pt oxides, as mentioned above.

4. Conclusions

We have presented a new experimental setup for the purpose of studying size-selected cluster deposition using XPS, STM, and a high-pressure reaction cell measurement. The high-pressure reaction cell measurement provided information on catalytic properties under conditions close to those in practical uses. STM measurements showed that soft-landing conditions were obtained. Catalytic activity measurements showed that the catalytic activities have a cluster-size dependence.

The geometries of Pt clusters on TiO₂ were revealed directly by atomic-resolution STM imaging. Clusters smaller than Pt₇ lay flat on the surface with a planar structure, and a planar-to-three-dimensional transition occurred at $n = 8$ for Pt_{*n*}.

The observed steep and gradual binding energy shifts with the cluster size could be understood in terms of

planar and 3D structures of the cluster geometries, respectively. Furthermore, the inflection point ($n = 8$) in the size dependence of the core-level shifts agrees well with the cluster size at a geometric transition (planar to 3D). It was found that the Pt core-level shifts for size-selected Pt clusters deposited on TiO₂ are closely correlated with cluster geometries determined directly by atomic-resolution STM imaging.

In future, the geometry of the clusters determined from atomic-resolution images is expected to be helpful in elucidating the origin of the observed cluster-size dependence in catalytic reactions and cluster-surface interactions. We are continuing research on the catalytic and electronic properties of size-selected clusters on metal oxide substrates from the viewpoint of cluster-support interaction, and we hope to devise a method for developing heterogeneous catalysts such as automotive exhaust catalysts.

Acknowledgments

We thank the late Professor Tamotsu Kondow and his co-workers (Toyota Technological Institute and Genesis Research Institute, Inc.) for their valuable comments during discussions. We also thank Dr. Shinichi Matsumoto, Mr. Mamoru Ishikiriyama, Mr. Hiroyuki Matsubara, Ms. Mayuko Osaki of Toyota Motor Corporation for their encouragement and help. We thank Professor M. Yoshimura of the Toyota Technological Institute for providing CNT tips for STM.

References

- (1) Heiz, U., Vanolli, F., Trento, L. and Schneider, W.-D., *Rev. Sci. Instrum.*, Vol.68 (1997), p.1986.
- (2) Heiz, U., *Appl. Phys. A: Mater. Sci. Process.*, Vol.67, No.6 (1998), p.621.
- (3) Heiz, U., Vanolli, F., Sanchez, A. and Schneider, W.-D., *J. Am. Chem. Soc.*, Vol.120 (1998), p.9668.
- (4) Lee, S., Fan, C., Wu, T., and Anderson, S., *J. Chem. Phys.*, Vol.123 (2005), p.124710.
- (5) Berlowitz, P. J., Peden, C. H. F. and Goodman, D. W., *J. Phys. Chem.*, Vol.92 (1988), p.5213.
- (6) Su, X., Cremer, P. S., Shen, Y. R. and Somorjai, G. A., *J. Am. Chem. Soc.*, Vol.119 (1997), p.3994.
- (7) Kveskin, S. J., Rioux, R. M., Habas, S. E., Komvopoulos, K., Yang, P. and Somorjai, G. A., *J. Phys. Chem. B*, Vol.110 (2006), p.15920.
- (8) Petrova, N. V. and Yakovkin, I. N., *Surf. Sci.*, Vol.578 (2005), p.162.
- (9) Tong, X., Benz, L., Kemper, P., Metiu, H., Bowers, M. T. and Buratto, S. K., *J. Am. Chem. Soc.*, Vol.127

- (2005), p.13516.
- (10) Piednoir, A., Perrot, E., Granjeaud, A., Humbert, S., Chapon, C. and Henry, C. R., *Surf. Sci.*, Vol.391 (1997), p.19.
- (11) Tait, R. H. and Kasowski, R. V., *Phys. Rev. B*, Vol.20 (1979), p.5178.
- (12) Henrich, V. E. and Kurtz, R. L., *Phys. Rev. B*, Vol.23 (1981) p.6280.
- (13) Göpel, W., Anderson, J. A., Frankel, D., Jaehnig, M., Phillips, K. J., Schäfer, A. and Rocker, G., *Surf. Sci.*, Vol.139 (1984), p.333.
- (14) Guo, Q., Lee, S. and Goodman, D. W., *Surf. Sci.*, Vol.437 (1999), p.38.
- (15) Onishi, H. and Iwasawa, Y., *Surf. Sci.*, Vol.313 (1994), p.L783.
- (16) Fischer, S., Munz, A.W., Schierbaum, K.-D. and Göpel, W., *Surf. Sci.*, Vol.337 (1995), p.17.
- (17) Isomura, N., Wu, X. and Watanabe, Y., *J. Chem. Phys.*, Vol.131 (2009), p.164707.
- (18) Watanabe, Y. and Isomura, N., *J. Vac. Sci. Technol. A*, Vol.27 (2009), p.1153.
- (19) Tanaka, K., Yoshimura, M. and Ueda, K., *e-J. Surf. Sci. Nanotech.*, Vol.4 (2006), p.276.
- (20) Tanaka, T., Yokota, K., Isomura, N., Doi, H. and Sugiura, M., *Appl. Catal. B: Environ.*, Vol.16 (1998), p.199.
- (21) Nagai, Y., Hirabayashi, T., Dohmae, K., Takagi, N., Minami, T., Shinjoh, H. and Matsumoto, S., *J. Catal.*, Vol.242 (2006), p.103.
- (22) Tauster, S. J., Fung, S. C., Baker, R. T. K. and Horsley, J. A., *Science*, Vol.211 (1981), p.1121.
- (23) Takasu, Y., Unwin, R., Tesche, B., Bradshaw, A. M. and Grunze, M., *Surf. Sci.*, Vol.77 (1978), p.219.
- (24) Mason, M. G., *Phys. Rev. B*, Vol.27 (1983), p.748.
- (25) Cheung, T. T. P., *Surf. Sci.*, Vol.127 (1983), p.L129.
- (26) Wertheim, G. K. and DiCenzo, S. B., *Phys. Rev. B*, Vol.37 (1988), p.844.
- (27) Luo, K., St. Clair, T. P., Lai, X. and Goodman, D. W., *J. Phys. Chem. B*, Vol.104 (2000), p.3050.
- (28) Heiz, U., Vanolli, F., Trento, L. and Schneider, W.-D., *Rev. Sci. Instrum.*, Vol.68 (1997), p.1986.
- (29) Eberhardt, W., Fayet, P., Cox, D. M., Fu, Z., Kaldor, A., Sherwood, R. and Sondericker, D., *Phys. Rev. Lett.*, Vol.64 (1990), p.780.
- (30) Fayet, P., Patthey, F., Roy, H.-V., Detzel, Th. and Schneider, W.-D., *Surf. Sci.*, Vol.269, Part B (1992), p.1101.
- (31) Kaden, W. E., Wu, T., Kunkel, W. A. and Anderson, S. L., *Science*, Vol.326 (2009), p.826.
- (32) Haberland, H., Karrais, M., Mall, M. and Thurner, Y., *J. Vac. Sci. Technol. A*, Vol.10 (1992), p.3266.
- (33) Shaffer, S. A., Tang, K., Anderson, G. A., Prior, D. C., Udseth, H. R. and Smith, R. D., *Rapid Commun. Mass Spectrom.*, Vol.11 (1997), p.1813.
- (34) Horcas, I., Fernandez, R., Gomez-Rodriguez, J., Colchero, M. J., Gomez-Herrero, J. and Baro, A. M., *Rev. Sci. Instrum.*, Vol.78 (2007), p.013705.
- (35) Carley, A. F., Chalker, P. R., Riviere, J. C. and Roberts, M. W., *J. Chem. Soc. Faraday Trans. 1*, Vol.83 (1987), p.351.
- (36) Onishi, H. and Iwasawa, Y., *Surf. Sci.*, Vol.313 (1994), p.L783.
- (37) Diebold, U., *Surf. Sci. Rep.*, Vol.48 (2003), p.53.
- (38) Wendt, S., Schaub, R., Matthiesen, J., Vestergaard, E., Wahlström, M., Rasmussen, D., Thostrup, P., Molina, L. M., Lægsgaard, E., Stensgaard, I., Hammer, B. and Besenbacher, F., *Surf. Sci.*, Vol.598 (2005), p.226.
- (39) Xiao, L. and Wang, L., *J. Phys. Chem. A*, Vol.108 (2004), p.8605.
- (40) Schoiswohl, J., Kresse, J., Surnev, S., Sock, M., Ramsey, M. G. and Netzer, F. P., *Phys. Rev. Lett.*, Vol.92 (2004), p.206103.
- (41) Fischer, S., Schierbaum, K. D. and Göpel, W., *Vacuum*, Vol.48 (1997), p.601.
- (42) Xiao, L. and Wang, L., *Chem. Phys. Lett.*, Vol.392 (2004), p.452.
- (43) Aizawa, M., Lee, S. and Anderson, S. L., *J. Chem. Phys.*, Vol.117 (2002), p.5001.
- (44) Egelhoff Jr., W. F. and Tibbetts, G. G., *Phys. Rev. B*, Vol.19 (1979), p.5028.
- (45) Barr, T. L., *J. Vac. Sci. Technol. A*, Vol.7 (1989), p.1677.
- (46) Peuchert, M. and Bonzel, H. P., *Surf. Sci.*, Vol.145 (1984), p.239.
- Figs. 1 and 4-7
Reprinted from *J. Vac. Sci. Technol. A*, Vol.27, No.5 (2009), pp.1153-1158, Watanabe, Y. and Isomura, N., A New Experimental Setup for High-pressure Catalytic Activity Measurements on Surface Deposited Mass-Selected Pt Clusters, Copyright 2009, with permission from American Vacuum Society.
- Figs. 2, 3 and 11
Reprinted from *J. Surf. Sci. Soc. Jpn.*, Vol.31, No.10 (2010), pp.537-542, Watanabe, Y., Hirata, H. and Isomura, N., Surface Chemistry of Mass-selected Precious Metal Clusters on Metal Oxide Surface, Copyright 2010, with permission from *Sur. Sci. Soc. Jpn.*
- Figs. 8-10
Reprinted from *J. Chem. Phys.*, Vol.131, No.16 (2009), pp.164707-1-4, Isomura, N., Wu, X. and Watanabe, Y., Atomic-resolution Imaging of Size-selected Platinum Clusters on TiO₂(110) Surfaces, Copyright 2009, with permission from American Institute of Physics.
- Figs. 12-14
Reprinted from *J. Vac. Sci. Technol. A*, Vol.28, No.5 (2010), pp.1141-1144, Isomura, N., Wu, X., Hirata, H. and Watanabe, Y., Cluster Size Dependence of Pt Core-level Shifts for Mass-selected Pt Clusters on TiO₂(110) Surfaces, Copyright 2010, with permission from American Vacuum Society.

Yoshihide Watanabe

Research Fields :

- Cluster science
- Surface science

Academic Degree : Dr. Eng.

Academic Societies :

- The Chemical Society of Japan
- The Surface Science Society of Japan



Hirohito Hirata*

Research Field :

- Automotive exhaust catalysts

Academic Degree : Dr. Eng.

Academic Society :

- Catalysis Society of Japan



Noritake Isomura

Research Fields :

- Cluster science
- Surface science

Academic Societies :

- The Chemical Society of Japan
- The Japan Society of Applied Physics



Xingyang Wu**

Research Field :

- Tribology

Academic Degree : Ph.D

*Toyota Motor Corporation

**Shanghai University